Inorganic Chemistry

Systematic Doping of Cobalt into Layered Manganese Oxide Sheets Substantially Enhances Water Oxidation Catalysis

Ian G. McKendry,[†,‡] Akila C. Thenuwara,[†,‡] Samantha L. Shumlas,[†,‡] Haowei Peng,[§,‡]
Yaroslav V. Aulin,[†,‡] Parameswara Rao Chinnam,[†] Eric Borguet,[†,‡] Daniel R. Strongin,[†,‡]
and Michael J. Zdilla*[,†,‡]

[†]Department of Chemistry, Temple University, Beury Hall, 1901 North 13th Street, Philadelphia, Pennsylvania 19122, United States
[‡]Center for the Computational Design of Functional Layered Materials (CCDM), Temple University, 1925 North 12th Street, Philadelphia, Pennsylvania 19122, United States
[§]Department of Physics, Temple University, 1925 North 12th Street, Philadelphia, Pennsylvania 19122, United States

S *Supporting Information*

ABSTRACT: The effect on the electrocatalytic oxygen evolution reaction (OER) of cobalt incorporation into the metal oxide sheets of the layered manganese oxide birnessite was investigated. Birnessite and cobalt-doped birnessite were characterized by X-ray diffraction (XRD), X-ray photoelectron spectroscopy (XPS), Raman spectroscopy, and conductivity measurements. A cobalt:manganese ratio of 1:2 resulted in the most active catalyst for the OER. In particular, the overpotential (η) for the OER was 420 mV, significantly lower than the η = 780 mV associated with birnessite in the absence of Co. Furthermore, the Tafel slope for Co/birnessite was 81 mV/dec, in comparison to a Tafel slope of greater than 200 mV/dec for birnessite. For chemical water oxidation catalysis, an 8-fold turnover number (TON) was achieved (h = 70 mmol of O_2/mol of metal). Density functional theory (DFT) calculations predict that cobalt modification of birnessite resulted in a raising of the valence band edge and occupation of that edge by holes with enhanced mobility during catalysis. Inclusion of extra cobalt beyond the ideal 1:2 ratio was detrimental to catalysis due to disruption of the layered structure of the birnessite phase.
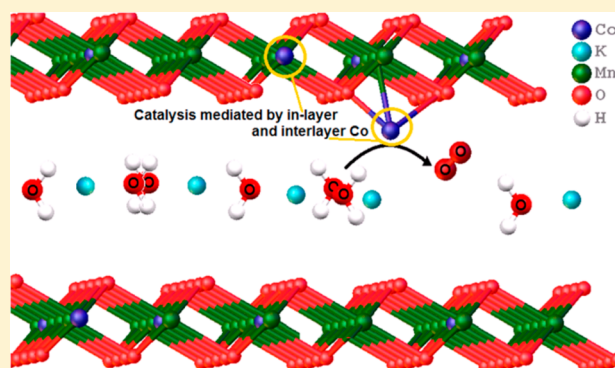
INTRODUCTION

The development of nonfossil-fuel-based alternative energy sources is of growing interest.[1] Storage of solar energy is often considered an ultimate goal due to its virtually unlimited supply. One appealing method is to store this energy chemically in the form of H_2, which can be obtained by splitting water:[2,3]

$$H_2O(l) \rightarrow 1/2 O_2(g) + H_2(g) \tag{1}$$
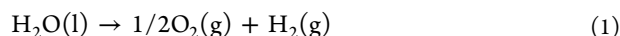
which has a standard free energy change, $\Delta G°$, of 237 kJ/mol. The oxygen evolution reaction (OER) is typically considered to be the most challenging part of water splitting since it requires the transfer of four electrons. In short, suitable, affordable OER catalysts must be developed and employed to make water splitting economically feasible.[3,4]

Layered manganese oxides have been under investigation for a number of applications due to their high surface to volume ratios, low cost, and topological and chemical similarities to the active site of photosystem II.[5] In recent years, much study has gone into birnessite as a potential candidate for the OER.[5−11] This material (Figure 1) is composed of edge-shared manganese oxide octahedra with interstitial cations to balance the overall negative charge of the layers resulting in inclusion of

Mn(III) sites into the mostly Mn(IV) sheets. These Mn(III) sites are believed to be an important active site feature in water oxidation catalysis.[12−18]

Several studies aimed at improving and exploiting these structural features have been reported.[12−14] The studies have shown a correlation between lower average manganese oxidation state and catalytic OER activity. This experimental observation stems from the paradigm of the importance of an occupied e_g valence orbital at the active site.[12−18]

In addition to identification of the active manganese species, the role of the interlayer cations has been investigated, and studies suggest that these interlayer ions may have a significant effect on catalytic activity as well.[9,12] Relevant to this report are recent computational studies by Lucht and Mendoza-Cortez on the effect of these intercalants and their role on electronic structure[17] and by Rao on the role of trivalent manganese.[18] Research from our own group has demonstrated that interlayer cations can enhance activity via providing catalytically active sites,[14,16] giving improved out-of-plane conductivity,[15] and
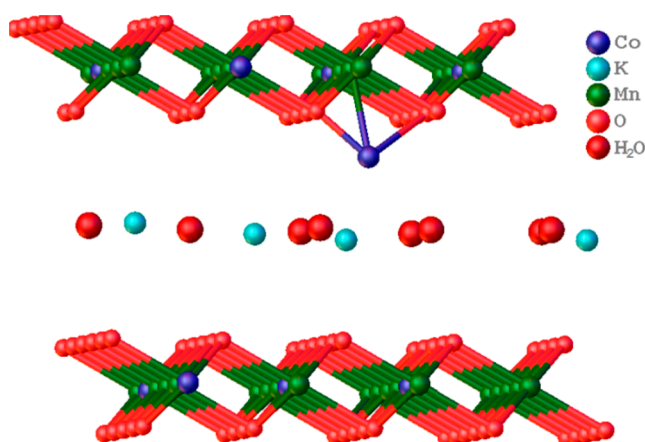
Figure 1. Hypothetical structure of cobalt-doped birnessite MnO_2 layers with interstitial cations with cobalt (purple), manganese (green), oxygen/water (red), and potassium (blue).

creating geometric frustration that enhances electron transfer rates.[16,19]

While significant research has been performed on the effects of geometric and electronic structure on the OER activity of birnessite, the effect of various in-layer (i.e., not interlayer) dopants[20,21] has not been explored for OER activity to our knowledge. In this study, we incorporate cobalt ions (another low-cost, high-activity redox-active transition metal) into birnessite. Here we investigate the degree to which cobalt can be incorporated into the structure and its effect on the OER activity of birnessite. DFT calculations support our experimental observations and provide insight into the role of Co in improving birnessite activity.

■ MATERIALS AND METHODS

General Considerations. All reagents were purchased from chemical vendors and used without further purification. X-ray diffraction (XRD) was performed on a Bruker D8 ADVANCE diffractometer using Cu Kα radiation from a sealed tube and processed using the DIFFRACEVA software package. Miller indices are indexed to the primitive Niggli reduced unit cell. Transmission electron microscopy (TEM) images were collected using a JEOL JEM-1400 microscope operating at 120 kV. Elemental mapping was performed using STEM-EDS. Scanning electron microscopy (SEM) samples were deposited on conductive carbon tape mounted on aluminum stubs and images collected on an Agilent 8500 FE-SEM instrument operating at 1 kV. X-ray photoelectron spectroscopy (XPS) was performed using a Thermo Fisher K-Alpha+ instrument with an Al Kα monochromatic X-ray source. Data collected for the Mn $2p_{3/2}$ and O 1s spectral regions were peak-fitted using Casa XPS software. To fit the Mn $2p_{3/2}$ region the procedure used by Nesbitt[22] was employed that takes into account the multiplet structure resulting from the presence of unpaired valence electrons in the 3d orbitals of manganese in the birnessite sample. This fitting procedure relies on the theoretical calculations by Gupta of the expected XPS spectra from the three Mn(IV), Mn(III), and Mn(II) ions. Prior work showed that the calculated XPS for the free ions (each containing five multiplet peaks) allowed the accurate fitting of experimental XPS Mn $2p_{3/2}$ data for birnessite. The contributions of the Mn(IV) to the XPS data were fitted with peaks at 642.15, 643.19, 644.0, 645.05, and 646.06 eV using a relative peak area ratio of 1:0.63:0.32:0.10:0.06. Mn(III) contributions to the XPS data were fitted with peaks at 640.83, 641.53, 642.34, 643.36, and 644.73 eV with a relative peak area ratio of 1.0:0.71:0.42:0.30:0.30. Peak area ratios for each Mn species were not changed during the fitting procedure. Peaks with a 50:50 Gaussian:Lorentzian contribution were used in the procedure, and the full width at half-maximum for each peak was 1.15 eV. Using these parameters the spectral data were

fitted by varying the relative contributions of individual sets of multiplet peaks.

Electrochemical measurements were performed with a CHI 660E electrochemical apparatus. Electrochemical studies were done in 1 M KOH with a glassy-carbon working electrode with values reported versus the standard hydrogen electrode (SHE). Inductively coupled plasma optical emission spectroscopy (ICP-OES) was performed to quantify elemental compositions using a Thermo Scientific iCAP 7000 Series ICP-OES instrument. Raman spectra were collected using a LabRAM HR Evolution spectrometer with a laser excitation wavelength of 532 nm and 1800 g/mm diffraction grating providing a spectral resolution of $\sim$1 cm^{-1}. Laser light was focused on an $\sim$1 μm spot with an Olympus MPlan N 100x objective. Excitation intensity was maintained below the damage threshold. Spectra were collected for at least three spots per sample to check the homogeneity of samples. Conductivity measurements were obtained on a Keithley 2400 Source-Meter SMU Instrument with four-probe setup.

Synthesis of Birnessite.[14,23] Hydrochloric acid (3 M, 50.0 mL) was added dropwise via a syringe pump at 1 mL/min to a heated and stirred (80 °C, 360 rpm) solution of potassium permanganate (0.200 M, 250 mL) in a 400 mL beaker. Heating was continued at 80 °C for an additional 0.5 h after addition of HCl was completed. The resulting 300 mL solution was then covered with a watch glass to prevent excessive evaporation and aged for 15 h at 50 °C before being filtered through a fine frit and washed five times with deionized water. The product was separated by centrifugation of the suspension in deionized water at 1000 rpm to remove any residual metal oxide nanoparticulate side products. Samples were dried by lyophilization.

Synthesis of Cobalt-Doped Birnessite. This synthesis was achieved via the same procedure as reported for birnessite above by addition of an additional 50 mL of $CoCl_2$ from stock solutions of varying concentration to give cobalt-doped birnessites. The samples prepared included the use of 50 mL each of 0.1 M (5 mmol) $CoCl_2$ to give $K_{0.16}Co_{0.12}Mn_{0.88}O_2$. 0.2 M (10 mmol) $CoCl_2$ for two samples, ($K_{0.15}Co_{0.21}Mn_{0.76}O_2$) and ($K_{0.19}Co_{0.22}Mn_{0.74}O_2$), 0.58 M (29 mmol) $CoCl_2$ for ($K_{0.08}Co_{0.28}Mn_{0.72}O_2$), and 1.1 M (55 mmol) $CoCl_2$ for ($K_{0.01}Co_{0.30}Mn_{0.70}O_2$). For higher Co loadings, the concentration of MnO_4^- in the initial solution was dropped from 0.200 to 0.080 M and 50 mL of 0.8 M $CoCl_2$ was added. When $CoCl_2$ solution was added dropwise simultaneously with the 50 mL of HCl solution, ($K_{0.05}Co_{0.38}Mn_{0.62}O_2$), was obtained. When the $CoCl_2$ solution was added to permanganate before addition of HCl ($K_{0.04}Co_{0.42}Mn_{0.58}O_2$) was obtained. The samples were dried by lyophilization.

Exfoliation of Nanosheets (NSs) for Analysis of Elemental Composition. The exfoliation of the $K_{0.01}Co_{0.30}Mn_{0.70}O_2$ sample was performed as previously reported[10] by stirring the powdered material in an aqueous tetra-n-butylammonium hydroxide (TBA$^+$OH$^-$; Aldrich Chemical Co., 40 wt % in H_2O) suspension for 3 days. The TBA$^+$OH$^-$ was isolated from the NSs and bulk by centrifugation at 14000 rpm for 30 min. The pellet containing the NSs and bulk was resuspended in water and washed by centrifugation at 14000 rpm for 30 min. The washing was repeated with ethanol and water as stated above. The pellet was then resuspended and centrifuged at 8000 rpm for 10 min, after which the dark blue-brown [$Co_{0.30}Mn_{0.70}O_2$] NS filtrate (colloidal suspension) was collected. Elemental analysis was performed using ICP-OES. The sample preparation of the $K_{0.01}Co_{0.30}Mn_{0.70}O_2$ NS suspension is as follows: 1.5 mL of the NS suspension was digested in 5 mL of oxalic acid (0.5 M). The solution was then diluted to 50 mL. Elemental analysis was also performed using TEM-EDS. One drop of the $K_{0.01}Co_{0.30}Mn_{0.70}O_2$ NS suspension was diluted to 2 mL, and the resulting solution was drop-casted onto a lacey carbon copper mesh TEM grid (Ted Pella, 400 mesh) and allowed to air dry.

Water Oxidation Activity. This activity was tested electrochemically using linear sweep voltammetry in 1 M KOH (pH 14) with a sweep rate of 10 mV/s. Overpotentials are reported at a current density of 10 mA cm^{-2}. The electrode was prepared by deposition of a catalyst ink, prepared by adding 4 mg of catalyst and 4 mg of carbon (VulcanXC-72), which was dispersed in 1 mL of isopropyl alcohol and 35 μL of Nafion solution (5% in alcohol, Ion Power Inc.). The resulting mixture was sonicated for at least 1 h to suspend particles

and form a catalyst ink. This was drop-casted on the electrode surface with a loading of 0.28 mg cm^{-2}. Chronopotentiometric experiments were performed at 5 and 10 mA cm^{-2}.

The O$_2$ yield from chemical water oxidation with ceric ion (0.04 M, 5 mL) was determined using a Hach HQ30d portable meter kit with LDO101 optical dissolved oxygen probe reading with a 1 mg/mL catalyst suspension in water. A suspension of approximately 15 mg of birnessite catalyst in 15 mL of water was degassed by bubbling N$_2$ or Ar through the solution while stirring for at least 3 h in a side arm flask. After this period, an N$_2$ blanket was applied to the flask through the side arm, and the O$_2$ probe was inserted through the neck of the flask. A 5 mL portion of argon-purged ammonium cerium(IV) nitrate (0.4 M, 2 mmol) was added to the suspension via a 10 mL syringe, and the O$_2$ was measured over time. The O$_2$ yield was normalized by total transition-metal content, as determined by ICP-OES, to give O$_2$ yield in units of mmol of O$_2$/mol of transition metal. The turnover number is calculated as the maximum height of the obtained normalized signal (Figure 7). The turnover frequency is calculated as the slope of the line fitted through the steepest ascent in the O$_2$ evolution plot near the start of the reaction (Figure S8 in the Supporting Information). TON and TOF are given normalized by moles of transition-metal ion in catalyst and by grams of catalyst (see the Supporting Information).

DFT Calculations. These calculations were performed using the projector augmented wave (PAW) method[24] as implemented in the VASP code.[25,26] The optB86b density functional[27] was used to approximate the exchange correlation, with an on-site Hubbard U of 3 eV for Mn and Co d states.[28] The c axis lattice constant was fixed to the experimental value, and a hexagonal lattice was always assumed. A 48-atom special quasi-random structure (SQS) was used to model the random alloy, mimicking the trivalent Mn(III) or Co(III) evenly distributed within the MnO$_2$ layers,[29] with K atoms intercalated for charge balance. A cutoff energy of 520 eV was chosen for the plane-wave basis, and a Monkhorst−Pack[30] $6 \times 6 \times 2$ k mesh was used to sample the Brillouin zone.

■ RESULTS

Characterization. XRD (Figure 2), TEM, SEM, and Raman techniques were used to characterize Co-birnessite and birnessite. While TEM and SEM (Figure 3 and Figures S2 and S3 in the Supporting Information) suggest that the birnessite morphology persisted irrespective of cobalt concentration, as evidenced by the flower pod morphology commonly observed in birnessite, XRD suggests a loss of order in the c (stacking) direction. The loss of crystallinity in the low-angle region has been previously observed and reported for Ni- and Co-doped birnessite.[20,31] The peak with no out-of-plane (l) contributions ($1\bar{1}0$ at 37°) is present in the
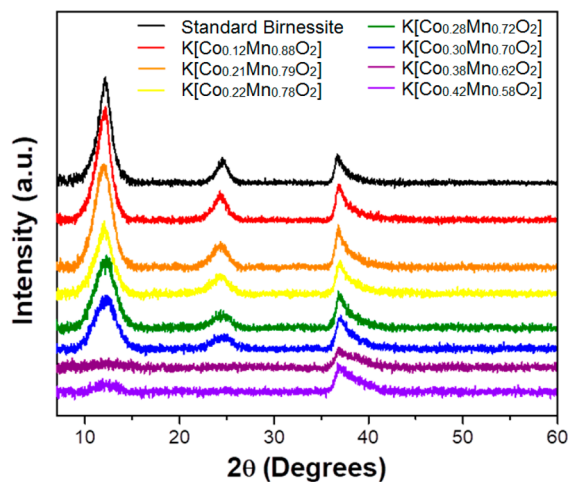

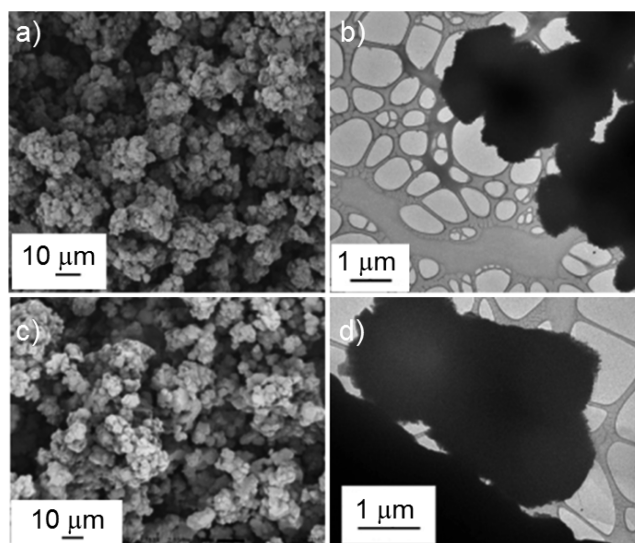**Figure 3.** Electron micrographs of pristine birnessite ((a) SEM, (b) TEM) and K{Co$_{0.38}$Mn$_{0.62}$O$_2$] ((c) SEM, (d) TEM).

diffractograms for all samples. However, the (001) and (002) peaks at 12.1 and 24.2° 2θ, corresponding to the stacking direction, decrease in intensity in samples containing >40% cobalt. This experimental observation suggests that the sheet morphology is maintained throughout the synthesis process, but that the order in the stacking direction decreases with increasing cobalt.

Birnessite is a mixed-valent manganese oxide containing Mn(III/IV) with an average oxidation state (AOS) typically close to 3.7. Mn(III) sites have been demonstrated by experiment to hold catalytic significance for manganese-mediated OER.[11−18] As such, the nature of the cobalt and manganese species in these samples is of particular interest in understanding the activity of Co-birnessite. EDS mapping studies (Figure S2 in the Supporting Information) demonstrates an even distribution of cobalt and manganese throughout the structure, while EDS and ICP of nanosheets exfoliated using tetrabutylamonium chloride treatment (Figures S3 and S9 and Table S3 in the Supporting Information) demonstrate the incorporation of cobalt into the 2D sheets. XPS (Figure 4 and Figure S1 in the Supporting Information) illustrates that Co(III) systematically replaces the Mn(III) in the birnessite samples. As the Mn(III) 2p$_{3/2}$ peaks in the Mn XPS spectrum decrease with increasing Co concentration, the Mn(IV) features remain. Increasing Co incorporation leads to an increase in the Co(III) 2p$_{3/2}$ XPS feature at 780 eV.[32,33] The absence of the Auger feature at 785 eV, which is characteristic of Co(II) XPS, suggests that low-spin Co(III) atoms are present in Co-birnessite. This phenomenon of preferential replacement of Mn(III), which has been observed previously,[34] leaves a lattice comprising exclusively Co(III) and Mn(IV) (Figure S1b,c). Solid-state magnetometry (Figure S6 in the Supporting Information) on these samples is consistent with the inclusion of Co within the sheets as evidenced by the Weiss constant (Θ), which is large and negative for pure birnessite but becomes increasingly positive with increased cobalt content. This behavior is consistent with decreased antiferromagnetic ordering at low temperature induced by the inclusion of S = 0 Co(III) ions, which disrupts the normal antiferromagnetic ordering of Mn(IV) sheets in pure birnessite.[35]

Figure 2. PXRD patterns of standard birnessite and cobalt-doped birnessite.
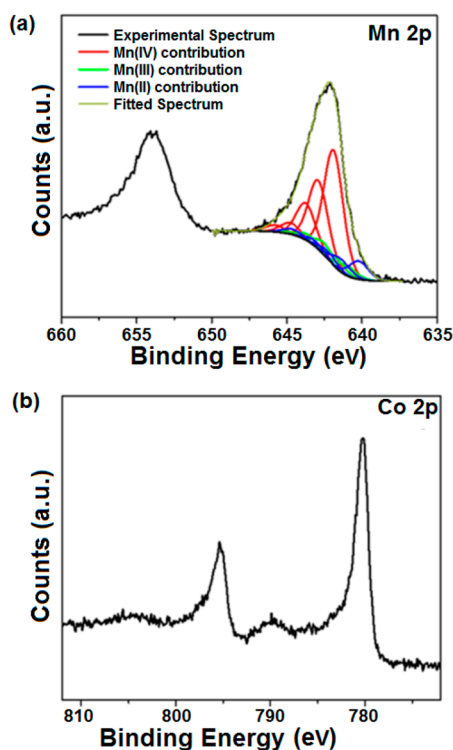
Figure 4. XPS spectra of (a) Mn 2p and (b) Co 2p. An analysis of the Mn $2p_{3/2}$ region indicates the major species are Mn(IV) and Co(III) with negligible amounts of Mn(III) and Mn(II).

Figure 5. Calculated density of states for (a) pure MnO_2, (b) $K_{0.25}MnO_2$, (c) $K_{0.125}Co_{0.125}Mn_{0.875}O_2$, and (d) $K_{0.25}Co_{0.25}Mn_{0.75}O_2$, illustrating the modification of electronic structure by Co incorporation. The energy axis is referenced to the Mn(IV)-dominated conduction band minimum.

In manganese oxide based water oxidation catalysts, the valence band edge lies significantly below the theoretical water oxidation potential,[4] requiring large overpotentials to inject holes into this band. The inclusion of electron-rich Mn(III) and Co(III) favorably alters the electronic structure in a similar way that raises the valence band edge, promoting catalysis.[17]

In Figure 5, we compared the electronic structure of pure MnO_2, $K_4Mn_{16}O_{32}$, $K_2Co_2Mn_{14}O_{32}$, and $K_4Co_4Mn_{12}O_{32}$ from DFT+U calculations. In pure MnO_2 (Figure 5a), the Mn(IV) ion has three d electrons fully occupying the majority-spin t_2 states contributing to the valence band, while the empty e_g states dominate the conduction band bottom. Alloying with Mn(III) (Figure 5b) develops a new valence band mainly composed of Mn(III) d_{z^2} states, derived from states analogous to those in the conduction band of the all Mn(IV) material. In contrast, the modification of the electronic structure by Co alloying mainly occurs near the original valence band edge (Figure 5c,d). The incorporated low-spin Co(III) has six d electrons fully occupying both the majority- and minority-spin t_2 orbitals. The same symmetry allows hybridization between the Co and Mn d states within the valence band, and we can see that the Co(III)-related bands are much more delocalized than the Mn(III)-related bands given the same concentration, as shown in Figure 5b,d. Hence, the inclusion of Co results in a more dispersive valence band edge, and the resulting holes have lower effective mass and therefore higher mobility. The observation is similar to that seen in Mn(III)-rich manganese oxide systems;[17,18] however, the effect is more pronounced in this Co-doped system in comparison to that observed in the common Mn(III)-containing systems.[15,17,18]

Quantification of Co as a function of reaction stoichiometry shows that the Co:Mn content ratio in the final product increases in a prop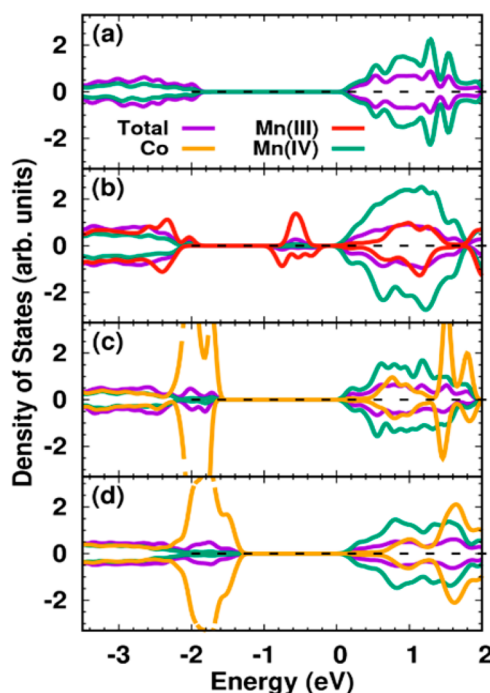ortion equivalent to the ratio of Co and Mn precursors in solution up to a saturation of 1:1. Beyond this point, inclusion of additional Co(II) in solution does not further enrich the birnessite with Co. We hypothesize that this maximum capacity for Co in the birnessite phase results from the increasing negative charge in the birnessite sheets as a result of a decrease in the proportion of tetravalent Mn(IV) cations and an increase in the concentration of trivalent Co(III) cations in the sheet structure. The increasing negative charge in the sheet requires an increase in interlayer cations to balance the charge. However, the interlayer of birnessite is already highly crowded by potassium ions,[16,19,36] possibly restricting the amount of negative charge in the sheet that can be balanced by potassium. However, this crowding of cations in the interlayer could be relieved by the inclusion of Co^{3+} ions in the interlayer as well, since Co^{3+} ions balance more charge than monovalent K^+. The hexagonal phase of birnessite under study here is known to possess this type of interlayer Mn ion defect in small amounts.[37] It is therefore plausible that, under increased Co loading conditions, additional Co^{3+} ions are trapped between the sheets during self-assembly and in doing so stabilize a greater level of Co incorporation into the sheet and the associated large negative charge therein. Thus, doping results both in Co occupancy within the sheet (increasing negative charge) and in the interlayer region (balancing this charge). This use of more charge dense species permits more charge to be localized in the interlayer: up to a total Co:Mn ratio of 1:1 overall. This hypothesis of Co doping into the interlayer is consistent with the increase in stacking disorder observed as a function of Co concentration (Figure 2).

To test this hypothesis, Raman spectroscopy was performed to obtain insight into the local structures through observations of M−O vibrational modes. Previous work has associated Raman peaks at ∼575 and ∼640 cm^{-1} the with the in- and out-of-plane Mn−O stretch of the birnessite sheet, respectively.[38]

The ratio of the two peaks remains the same up to 24% Co incorporation, suggesting that cobalt substitution is primarily occurring within the sheet. Above 24% substitution, the ratio of the intensities of the in-plane to out-of-plane stretch[34,38] decreases with the incorporation of cobalt in the interlayer region (Figure 6). This same behavior was observed previously when Ni^{2+} and Co^{2+} were incorporated into the interlayer of standard birnessite.[19,36] An almost identical behavior is seen in conductivity measurements (Figure S10 in the Supporting Information), where the conductivity of the sample remains constant up to 24% Co incorporation but drops beyond this point, suggesting a disruption of interlayer electronic communication imposed by the stacking disorder. The Raman spectra, conductivity, and XRD are all consistent with a disruption of order in the stacking direction by excessive interlayer cobalt inclusion.

Catalytic Activity. Birnessites with and without incorporated Co were tested for OER activity by using the material as an anode in electrochemical experiments and by exposing the catalyst to a chemical oxidant (ceric ammonium nitrate). The results of these experiments are illustrated in Figure 7. Increasing cobalt content is correlated with improved electrocatalytic activity under basic conditions: The overpotential and Tafel slope are both improved up to about a 1:2 Co:Mn ratio, at which point the overpotential had decreased from $\eta = 780$ (no cobalt) to 420 mV. The Tafel slope, b, decreased from 250 to 81 mV/dec (Table 1). These results, therefore, showed a 360 mV reduction in overpotential and 70% reduction in Tafel slope at a 33% Co incorporation. It is worthwhile to note from the characterization data from Tables S1−S6 in the Supporting Information that the catalytic activity correlates best with cobalt content, rather than other parameters such as Mn(III) content, surface area, and interlayer water content. Chronopotentiometric experiments at 5 mA cm^{-2} (Figure S7 in the Supporting Information) show stability of the best catalysts for greater than 4 h. Chronopotentiometry at 10 mA cm^{-2} shows the stability of the best catalysts for 2−3 h (Figure 7).

Similarly, chemical oxidation in the presence of ceric ion under acidic conditions (Figure 6 and Table 1) showed a similar trend. Standard birnessite shows catalytic activity comparable to
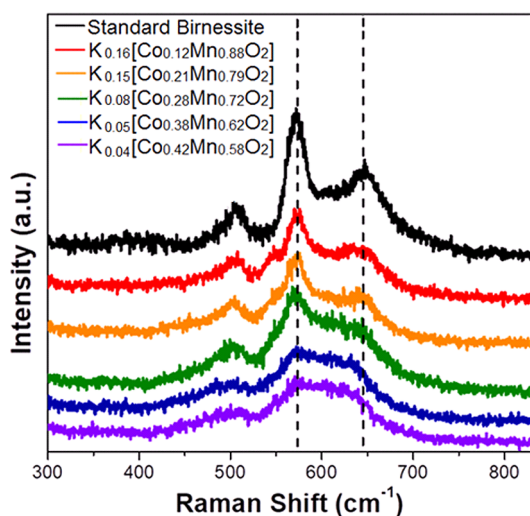
Figure 7. Water oxidation activity of catalysts. (a) Linear sweep voltammetry (10 mV/s). (b) Chronopotentiometry at 10 mA cm^{-2}. Sharp jumps in plot result from the formation and escape of O_2 bubbles on the electrode. (c) Ceric ion oxidation of water catalyzed by doped birnessites with vertical axis normalized by total moles of transition metal (Co + Mn) content in the bulk.

those previously reported,[9,14] evolving O_2 for 1−2 h. The highest performing birnessite, while only functioning about 30 min, showed significant activity improvement. Increased OER rate and turnover was seen with increasing cobalt content up to 33%, with $K[Co_{0.34}Mn_{0.76}O_2]$ possessing the greatest activity, with a turnover number (TON) of 70 mmol of O_2/mol of metal in comparison to pristine birnessite with values of 8.8 mmol O_2/mol transition metal: an 8-fold increase in TON. In all experiments inclusion of additional cobalt content past 33% resulted in a worsening of the catalytic performance.

Figure 6. Raman spectra of cobalt-doped birnessite samples as a function of percent cobalt content. The ratio of the intensity between in-plane (570 cm^{-1}) and out-of-plane stretch (635 cm^{-1}) decreases with increasing cobalt content above 24% (see also Figure S9 in the Supporting Information). See also Figure S10.
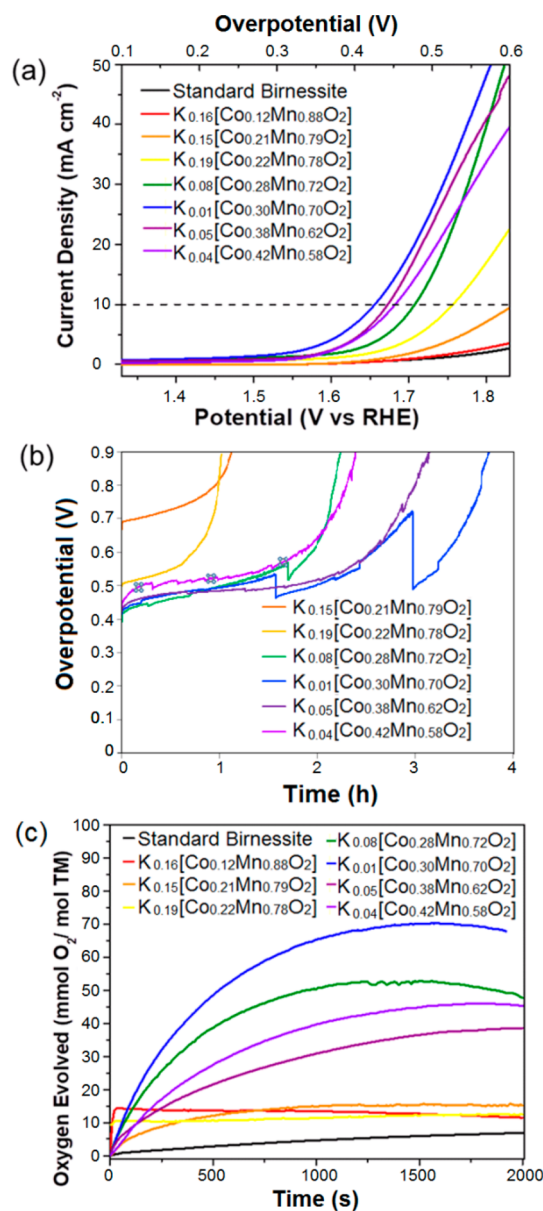
■ DISCUSSION AND CONCLUSION

The enhancement of OER activity via Co incorporation is understandable in light of a number of considerations. (1) An increase in overall charge of the sheet has been associated with

Table 1. Summary of Catalyst Activity by Electrochemistry and Chemical Oxidation

sample	η (mV)[a]	Tafel slope (mV/dec)[a]	TON[b,c] (mmol of O_2/mol of TM)
birnessite	780	240	8.8
$K_{0.16}[Co_{0.12}Mn_{0.88}O_2]$	750	230	9.2
$K_{0.15}[Co_{0.20}Mn_{0.76}O_2]$	600	180	13
$K_{0.19}[Co_{0.22}Mn_{0.78}O_2]$	525	100	16
$K_{0.08}[Co_{0.28}Mn_{0.72}O_2]$	475	92	53
$K_{0.01}[Co_{0.30}Mn_{0.70}O_2]$	425	81	70
$K_{0.05}[Co_{0.38}Mn_{0.62}O_2]$	470	110	46
$K_{0.04}[Co_{0.42}Mn_{0.58}O_2]$	450	110	38

[a]Conditions: pH 14, LSV, sweep rate 10 mV/s. [b]Conditions: pH 2, $[Ce^{4+}]_0$ = 40 mM. [c]Calculated from highest point on O_2 evolution plot (Figure 7c).

enhanced geometric frustration of the substrate water molecules, which lowers the reorganization energies associated with electron transfer, increasing the rate of catalysis.[16] Inclusion of highly Lewis acidic Co^{3+} ions should result in further enhancement of this effect. (2) Defect sites such as the corner-shared interlayer transition-metal ion proposed here have been implicated as the active sites in birnessite water oxidation.[11,14,37] These species may serve a role in favorably altering the band structure of the catalyst or by serving as a catalytically active site, lowering the energy of catalytic transition states. For instance, past work on intercalation of Ni or Co into the interlayer (but not into the sheets) of Mn-only birnessite gave catalysts where the interlayer cation acts as the catalyst.[19,36] Combining arguments (1) and (2) above, inclusion of such active transition-metal ion catalysts in the dynamically enhanced interlayer of birnessite can have a synergistic effect in promoting catalytic activity.[36] (3) The inclusion of small amounts of transition-metal ions between the sheets increases the out-of-plane conductivity by bridging the sheets, permitting more facile charge transport between the material and the electrode surface.[15,36] (4) The addition of cobalt raises the energy of the valence band edge, decreasing the overpotential required to generate holes in the electrocatalyst. (5) The calculated density of states suggests dispersive bands and high-mobility holes for the cobalt-containing structures. These features all contribute to the improvement of a very poor catalyst—birnessite—by improving the kinetics of electron transfer, promoting long-range conductivity, introducing catalytic active sites, and decreasing the activation barrier to catalyst oxidation. However, results from XRD, Raman, and conductivity measurements show that overincorporation of Co disrupts the stacking structure of the material, decreasing the ordering in the crystallographic c direction and decreasing conductivity (presumably in the c direction). While small amounts of intercalants increase both conductivity and stacking order (based on XRD) in birnessite,[15,36] higher levels of incorporation above 33% result in overcrowding that appears to disrupt the stacking and the conductivity. These detrimental effects overcome the beneficial effects of in-layer and interlayer cobalt incorporation. As a result, the optimal incorporation level of Co into birnessite is 33%, a concentration at which the conductivity, geometric-frustration-enhanced electron transfer rates, and density of active sites are optimized without compromising the birnessite structure.

Here we report a simple and inexpensive way to improve layered manganese oxide catalysts in terms of both reducing overpotential (by 360 mV) and increasing turnover number (8×) through the incorporation of Co(III) as an in-layer and interlayer dopant. The improvement in catalysis is explainable by a combination of features in this catalyst from prior work,[14–16,19,36] including enhanced bulk conductivity, enhanced local electron transfer kinetics, introduction of defect active sites, and kinetic enhancement of the rate-limiting mechanistic steps of those active sites. These well-known features in combination with new results predicting a raising of the valence band edge toward the thermodynamic water oxidation potential are additive, resulting in a system superior to the parent phase and competitive with excellent water oxidation catalysts previously reported but not competitive with iridium oxide or double-layer hydroxide catalysts.[39–41]

■ ASSOCIATED CONTENT

Ⓢ Supporting Information

The Supporting Information is available free of charge on the ACS Publications website at DOI: 10.1021/acs.inorgchem.7b01592.

> XPS, TEM, SEM, EDS, magnetic data, chronoamperometry, kinetic determination of TOF and TON, analysis of Raman data, conductivity measurements, average oxidation state determination, and BET surface area measurements (PDF)

■ AUTHOR INFORMATION

Corresponding Author

*E-mail for M.J.Z.: mzdilla@temple.edu.

ORCID Ⓞ

Akila C. Thenuwara: 0000-0002-6146-9238
Yaroslav V. Aulin: 0000-0002-7370-1241
Daniel R. Strongin: 0000-0002-1776-5574
Michael J. Zdilla: 0000-0003-0212-2557

Notes

The authors declare no competing financial interest.

■ ACKNOWLEDGMENTS

■ ABBREVIATIONS

TON,turnover number; TOF,turnover frequency; OER,oxygen evolution reaction; PXRD,powder X-ray diffraction; XRD,X-ray diffraction; XPS,X-ray photoelectron spectroscopy; TEM,transmission electron microscopy; EDS,energy dispersive spectroscopy; SEM,scanning electron microscopy; ICP-OES,inductively coupled plasma optical emission spectroscopy.

■ REFERENCES

(1) Walter, M. G.; Warren, E. L.; McKone, J. F.; Boettcher, S. W.; Mi, Q.; Santon, E. A.; Lewis, N. S. Solar Water Splitting Cells. *Chem. Rev.* **2010**, *110*, 6446.

(2) Bak, T.; Nowotny, J.; Rekas, M.; Sorrell, C. C. Photo-electrochemical hydrogen generation from water using solar energy. *Int. J. Hydrogen Energy* **2002**, *27*, 991.

(3) Koper, M. T. M. Thermodynamic theory of multi-electron transfer reactions. *J. Electroanal. Chem.* **2011**, *660*, 254.

(4) Pinaud, B. A.; Chen, Z.; Abram, D. N.; Jaramillo, T. F. Thin Films of Sodium Birnessite-Type MnO2: Optical Properties, Electronic Band Structure, and Solar Photoelectrochemistry. *J. Phys. Chem. C* **2011**, *115*, 11830.

(5) Zaharieva, I.; Najafpour, M. M.; Wiechen, M.; Haumann, M.; Kurz, P.; Dau, H. Synthetic manganese-calcium oxides mimic the water-oxidizing complex of photosynthesis functionally and structurally. *Energy Environ. Sci.* **2011**, *4*, 2400.

(6) Frey, C. E.; Wiechen, M.; Kurz, P. Water-oxidation catalysis by synthetic manganese oxides - systematic variations of the calcium birnessite theme. *Dalton Trans.* **2014**, *43*, 4370.

(7) Birkner, N.; Nayeri, S.; Pashaei, B.; Najafpour, M. M.; Casey, W. H.; Navrotsky, A. Energetic basis of catalytic activity of layered nanophase calcium manganese oxides for water oxidation. *Proc. Natl. Acad. Sci. U. S. A.* **2013**, *110*, 8801.

(8) Kwon, K. D.; Refson, K.; Sposito, G. On the role of Mn(IV) vacancies in the photoreductive dissolution of hexagonal birnessite. *Geochim. Cosmochim. Acta* **2009**, *73*, 4142.

(9) Wiechen, M.; Zaharieva, I.; Dau, H.; Kurz, P. Layered manganese oxides for water-oxidation: alkaline earth cations influence catalytic activity in a photosystem II-like fashion. *Chem. Sci.* **2012**, *3*, 2330.

(10) Kang, Q.; Vernisse, L.; Remsing, R. C.; Thenuwara, A. C.; Shumlas, S. L.; McKendry, I. G.; Klein, M. L.; Borguet, E.; Zdilla, M. J.; Strongin, D. R. Effect of Interlayer Spacing on the Activity of Layered Manganese Oxide Bilayer Catalysts for the Oxygen Evolution Reaction. *J. Am. Chem. Soc.* **2017**, *139*, 1863.

(11) Robinson, D. M.; Go, Y. B.; Mui, M.; Gardner, G.; Zhang, Z.; Mastrogiovanni, D.; Garfunckel, E.; Li, J.; Greenblatt, M.; Dismukes, G. C. Effect of Interlayer Spacing on the Activity of Layered Manganese Oxide Bilayer Catalysts for the Oxygen Evolution Reaction. *J. Am. Chem. Soc.* **2013**, *135*, 3494.

(12) Najafpour, M. M.; Isaloo, M. A.; Ghobadi, M. Z.; Amini, E.; Haghihi, B. The effect of different metal ions between nanolayers of manganese oxide on water oxidation. *J. Photochem. Photobiol., B* **2014**, *141*, 247.

(13) Takashima, T.; Hashimoto, K.; Nakamura, R. Mechanisms of pH-Dependent Activity for Water Oxidation to Molecular Oxygen by MnO2 Electrocatalyst. *J. Am. Chem. Soc.* **2012**, *134*, 1519.

(14) McKendry, I. G.; Kondaveeti, S. K.; Shumlas, S. L.; Strongin, D. R.; Zdilla, M. J. Decoration of the layered manganese oxide birnessite with Mn(II/III) gives a new water oxidation catalyst with fifty-fold turnover number enhancement. *Dalton Trans.* **2015**, *44*, 12981.

(15) Thenuwara, A. C.; Shumlas, S. L.; Attankayake, N. H.; Cerkez, E. B.; McKendry, I. G.; Frazer, L.; Borguet, E.; Kang, Q.; Zdilla, M. J.; Sun, J.; Strongin, D. R. Copper-Intercalated Birnessite as a Water Oxidation Catalyst. *Langmuir* **2015**, *31*, 12807.

(16) Remsing, R. C.; McKendry, I. G.; Strongin, D. R.; Zdilla, M. J. Frustrated Solvation Structures Can Enhance Electron Transfer Rates. *J. Phys. Chem. Lett.* **2015**, *6*, 4804.

(17) Lucht, K. P.; Mendoza-Cortes, J. L. Birnessite: A Layered Manganese Oxide To Capture Sunlight for Water-Splitting Catalysis. *J. Phys. Chem. C* **2015**, *119*, 22838.

(18) Maitra, U.; Naidu, B. S.; Govindaraj, A.; Rao, C. N. R. Importance of trivalency and the e(g)(1) configuration in the photocatalytic oxidation of water by Mn and Co oxides. *Proc. Natl. Acad. Sci. U. S. A.* **2013**, *110*, 11704.

(19) Thenuwara, A. C.; Cerkez, E. B.; Shumlas, S. L.; Attanayake, N. H.; McKendry, I. G.; Frazer, L.; Borguet, E.; Kang, Q.; Remsing, R. C.; Klein, M. L.; Zdilla, M. J.; Strongin, D. R. Nickel Confined in the Interlayer Region of Birnessite: an Active Electrocatalyst for Water Oxidation. *Angew. Chem., Int. Ed.* **2016**, *55*, 10381.

(20) Yin, H.; Wang, Y.; Ginder-Vogel, M.; Qiu, G.; Feng, X.; Zheng, L.; Liu, F. Effects of Co and Ni co-doping on the structure and reactivity of hexagonal birnessite. *Chem. Geol.* **2014**, *381*, 10.

(21) Yin, H.; Feng, X.; Qui, G.; Tan, W.; Liu, F. Characterization of Co-doped birnessites and application for removal of lead and arsenite. *J. Hazard. Mater.* **2011**, *188*, 341.

(22) Nesbitt, H. W.; Banerjee, D. Interpretation of XPS Mn(2p) spectra of Mn oxyhydroxides and constraints on the mechanism of MnO2 precipitation. *Am. Mineral.* **1998**, *83*, 305−315.

(23) McKenzie, R. M. The Synthesis of Birnessite, Cryptomelane, and Some Other Oxides and Hydroxides of Manganese. *Mineral. Mag.* **1971**, *38*, 493−502.

(24) Blöchl, P. E. Projector augmented-wave method. *Phys. Rev. B: Condens. Matter Mater. Phys.* **1994**, *50*, 17953.

(25) Kresse, G.; Hafner, I. Ab initio molecular-dynamics simulation of the liquid-metal−amorphous-semiconductor transition in germanium. *Phys. Rev. B: Condens. Matter Mater. Phys.* **1994**, *49*, 14251.

(26) Kresse, G.; Furthmüller, I. Efficient iterative schemes for ab initio total-energy calculations using a plane-wave basis set. *Phys. Rev. B: Condens. Matter Mater. Phys.* **1996**, *54*, 11169.

(27) Kresse, G.; Joubert, D. From ultrasoft pseudopotentials to the projector augmented-wave method. *Phys. Rev. B: Condens. Matter Mater. Phys.* **1999**, *59*, 1758.

(28) Dudarev, S. L.; Botton, G. A.; Savrasov, S. Y.; Humphreys, C. J.; Sutton, A. P. Electron-energy-loss spectra and the structural stability of nickel oxide: An LSDA+U study. *Phys. Rev. B: Condens. Matter Mater. Phys.* **1998**, *57*, 1505.

(29) Zunger, A.; Wei, S.; Ferreira, J.; Bernard, J. Special quasirandom structures. *Phys. Rev. Lett.* **1990**, *65*, 353.

(30) Monkhorst, H.; Pack, J. Special points for Brillouin-zone integrations. *Phys. Rev. B* **1976**, *13*, 5188.

(31) Yin, H.; Tan, H.; Zheng, L.; Cui, H.; Qiu, G.; Liu, F.; Feng, X. Characterization of Ni-rich hexagonal birnessite and its geochemical effects on aqueous Pb2+/Zn2+ and As(III). *Geochim. Cosmochim. Acta* **2012**, *93*, 47.

(32) Nesbitt, H. W.; Canning, G. W.; Bancroft, G. M. XPS study of reductive dissolution of 7 angstrom-birnessite by H3AsO3, with constraints on reaction mechanism. *Geochim. Cosmochim. Acta* **1998**, *62*, 2097.

(33) Biesinger, M. C.; Payne, B. P.; Grosvenor, A. P.; Lau, L. W. M.; Gerson, A. R.; Smart, R. S. C. Resolving surface chemical states in XPS analysis of first row transition metals, oxides and hydroxides: Cr, Mn, Fe, Co and Ni. *Appl. Surf. Sci.* **2011**, *257*, 2717.

(34) Julien, C.; Massot, M.; Baddour-Hadjean, R.; Franger, S.; Bach, S.; Pereira-Ramos, J. − P. Raman spectra of birnessite manganese dioxides. *Solid State Ionics* **2003**, *159*, 345.

(35) Kan, M.; Zhou, J.; Sun, Q.; Kawazoe, Y.; Jena, P. The Intrinsic Ferromagnetism in a MnO2Monolayer. *J. Phys. Chem. Lett.* **2013**, *4* (20), 3382−3386.

(36) Thenuwara, A. C.; Shumlas, S. L.; Attanayake, N. H.; Aulin, Y. V.; McKendry, I. G.; Qiao, Q.; Zhu, Y.; Borguet, E.; Zdilla, M. J.; Strongin, D. R. Intercalation of cobalt into the interlayer of birnessite improves oxygen evolution catalysis. *ACS Catal.* **2016**, *6*, 7739.

(37) Smith, P. F.; Deibert, B. J.; Kaushik, S.; Gardner, G.; Hwang, S.; Wang, H.; Al-Sharab, J. F.; Garfunkel, E.; Fabris, L.; Li, J.; Dismukes, G. C. Coordination Geometry and Oxidation State Requirements of Corner-Sharing MnO6 Octahedra for Water Oxidation Catalysis: An

Investigation of Manganite (gamma-MnOOH). *ACS Catal.* **2016**, *6*, 2089.

(38) Ogata, A.; Komaba, S.; Baddour-Hadjean, B.; Pereira-Ramos, J. − P.; Kumagai, N. Doping effects on structure and electrode performance of K-birnessite-type manganese dioxides for rechargeable lithium battery. *Electrochim. Acta* **2008**, *53*, 3084.

(39) Shao, M.; Zhang, R.; Li, Z.; Wei, M.; Evans, D. G.; Duan, X. Layered double hydroxides toward electrochemical energy storage and conversion: design, synthesis and applications. *Chem. Commun.* **2015**, *51*, 15880.

(40) McCrory, C. C. L.; Jung, S.; Peters, J. C.; Jaramillo, T. F. Benchmarking Heterogeneous Electrocatalysts for the Oxygen Evolution Reaction. *J. Am. Chem. Soc.* **2013**, *135*, 16977.

(41) Gao, M.; Sheng, W.; Zhuang, Z.; Fang, Q.; Gu, S.; Jiang, J.; Yan, Y. Efficient Water Oxidation Using Nanostructured alpha-Nickel-Hydroxide as an Electrocatalyst. *J. Am. Chem. Soc.* **2014**, *136*, 7077.